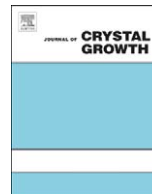




ELSEVIER

Contents lists available at ScienceDirect

Journal of Crystal Growth

journal homepage: www.elsevier.com/locate/jcrysgr

Characterization of bulk GaN crystals grown from solution at near atmospheric pressure

N.Y. Garces^{a,*}, B.N. Feigelson^a, J.A. Freitas Jr^a, Jihyun Kim^b, R.L. Myers-Ward^a, E.R. Glaser^a

^a Naval Research Laboratory, Codes 6877, 6882, Washington, DC 20375, United States

^b Department of Chemical and Biological Engineering, Korea University, Seoul, Korea

ARTICLE INFO

Keywords:

A1. Characterization

B1. Nitrides

B2. Semiconducting III–V materials

ABSTRACT

The properties of GaN crystals grown from solution at temperatures ranging from 780 to 810 °C and near atmospheric pressure ~ 0.14 MPa, have been investigated using low temperature X-band (~ 9.5 GHz) electron paramagnetic resonance spectroscopy, micro-Raman spectroscopy, photoluminescence spectroscopy, and photoluminescence imaging. Our samples are spontaneously nucleated thin platelets of approximate dimensions of $2 \times 2 \times 0.025$ mm³, or samples grown on both polycrystalline and single crystal HVPE large-area ($\sim 3 \times 8 \times 0.5$ mm³) seeds. Electron paramagnetic resonance spectra consists of a single Lorentzian line with axial symmetry about the *c*-axis, with approximate *g*-values, $g_{\parallel} = 1.951$ and $g_{\perp} = 1.948$ and a peak-to-peak linewidth of ~ 4.0 G. This resonance has been previously assigned to shallow impurity donors/conduction electrons in GaN and attributed to Si- and/or O impurities. Room temperature photoluminescence and photoluminescence imaging data from both Ga- and N-faces show different dominant emission bands, suggesting different incorporation of impurities and/or native defects. Raman scattering and X-ray diffraction show moderate to good crystalline quality.

© 2010 Elsevier B.V. All rights reserved.

1. Introduction

GaN continues to be one of the most attractive and important wide-band-gap semiconductor material systems. Its multitude of applications in electronics, optoelectronics, and new developments in epitaxial and bulk crystal growth techniques are topics of on-going research. Depending on the growth method, GaN crystals contain different levels of impurities and structural defects governing its optical and electronic properties. The availability of high-quality large-area free-standing substrates at low cost is essential for the GaN industrial progress. In particular, for high efficiency light emitting diodes (LEDs) and green laser applications, high-quality substrates with controlled optoelectronic properties are needed. Great progress has been achieved in the growth of large bulk *c*-plane GaN substrates by the ammonothermal method, with crystal sizes in the 1–2 in diameter range and thicknesses up to ~ 14 mm, and a relatively small concentration of threading-dislocation densities ($\sim 10^4$ cm⁻²) [1]. In addition, these substrates show excellent crystalline quality where very narrow X-ray rocking curves and full width at half maximum (FWHM) values of ~ 16 and 18 arcsec

for the symmetrical and asymmetrical peaks, respectively, have been realized.

Typical growth rates for the ammonothermal method are ~ 20 – 30 $\mu\text{m}/\text{day}$, thus requiring several weeks to grow larger crystals and multiple reactors to satisfy a steady demand for substrates. Initially, the crystals were grown on foreign substrates, but that necessity is no longer required and the growth is currently done on ammono seeds [2]. One of the most common and successful approaches to GaN crystal growth to date is by the hydride vapor phase epitaxy (HVPE) technique. This quasi-bulk method allows growth of thick GaN films on foreign substrates such as sapphire or GaAs with growth rates as high as a few hundred microns per hour. Current large-area free-standing substrates have dislocation densities in the low to mid 10^6 cm⁻² [3]. However, HVPE GaN often has undesirable levels of residual donor impurities that lead to high net free carrier concentrations in the order of 10^{17} – 10^{18} electrons/cm⁻³, rendering the substrates n-type, suitable only for certain applications. Another approach to bulk GaN crystal growth is by the high-pressure/high-temperature solution method [4]. The crystals obtained by this technique have extremely low dislocation densities ($\sim 10^2$ cm⁻²) and highly uniform electrical conductivity. However, due to the low solubility of N in the liquid Ga metal, only crystals of ~ 0.045 cm² area are obtained. To mitigate this problem, large-area, 1–2 in diameter HVPE substrates are being used as seeds for high-pressure growth. The crystals can be grown

* Corresponding author. Fax: +1 202 767 1165.

E-mail addresses: garces@bloch.nrl.navy.mil (N.Y. Garces), jhyun7@korea.ac.kr (J. Kim).

Report Documentation Page

Form Approved
OMB No. 0704-0188

Public reporting burden for the collection of information is estimated to average 1 hour per response, including the time for reviewing instructions, searching existing data sources, gathering and maintaining the data needed, and completing and reviewing the collection of information. Send comments regarding this burden estimate or any other aspect of this collection of information, including suggestions for reducing this burden, to Washington Headquarters Services, Directorate for Information Operations and Reports, 1215 Jefferson Davis Highway, Suite 1204, Arlington VA 22202-4302. Respondents should be aware that notwithstanding any other provision of law, no person shall be subject to a penalty for failing to comply with a collection of information if it does not display a currently valid OMB control number.

1. REPORT DATE 2010		2. REPORT TYPE		3. DATES COVERED 00-00-2010 to 00-00-2010	
4. TITLE AND SUBTITLE Characterization of bulk GaN crystals grown from solution at near atmospheric pressure				5a. CONTRACT NUMBER	
				5b. GRANT NUMBER	
				5c. PROGRAM ELEMENT NUMBER	
6. AUTHOR(S)				5d. PROJECT NUMBER	
				5e. TASK NUMBER	
				5f. WORK UNIT NUMBER	
7. PERFORMING ORGANIZATION NAME(S) AND ADDRESS(ES) Naval Research Laboratory, Codes 6877, 6882, Washington, DC, 20375				8. PERFORMING ORGANIZATION REPORT NUMBER	
9. SPONSORING/MONITORING AGENCY NAME(S) AND ADDRESS(ES)				10. SPONSOR/MONITOR'S ACRONYM(S)	
				11. SPONSOR/MONITOR'S REPORT NUMBER(S)	
12. DISTRIBUTION/AVAILABILITY STATEMENT Approved for public release; distribution unlimited					
13. SUPPLEMENTARY NOTES					
14. ABSTRACT see report					
15. SUBJECT TERMS					
16. SECURITY CLASSIFICATION OF:			17. LIMITATION OF ABSTRACT	18. NUMBER OF PAGES	19a. NAME OF RESPONSIBLE PERSON
a. REPORT unclassified	b. ABSTRACT unclassified	c. THIS PAGE unclassified			

on one or both sides of the seeds and subsequently removed from it by polishing or sawing to obtain free-standing, highly conductive GaN substrates for laser applications [5].

In this article, we report on a study of the optical and electrical properties of GaN crystals grown by the near atmospheric pressure solution growth technique [6]. We used electron paramagnetic resonance (EPR) spectroscopy, micro-Raman spectroscopy, photoluminescence (PL) spectroscopy, and PL-imaging to characterize free-standing unintentionally doped single crystals. Single crystal X-ray diffraction (XRD) and secondary ion mass spectroscopy (SIMS) results on arbitrarily selected samples from the same growth batch are also included to complement our characterization effort.

2. Experimental

Single crystal GaN samples were grown using a solution technique that employs variations of a multi-component solvent to dissolve the GaN source. The samples were grown near 800 °C and at pressures < 0.2 MPa. A detailed description of the growth process is given in Ref. [6] and references therein. Unintentionally doped, seeded, and spontaneously nucleated single crystals of various sizes and thicknesses were obtained with this growth method.

Both free-standing (FS) spontaneously nucleated and seeded samples were studied, while only results for the spontaneously nucleated samples will be presented here. Characterization was performed on a selection of bulk GaN platelets ranging in sizes from 4 to 6 mm² in area and 0.025–0.04 mm in thickness. EPR data were taken at 10 K in a Bruker EMX spectrometer operating near 9.5 GHz (X-band) equipped with a liquid helium gas flow system for temperature control. The samples were placed in a quartz holder and inserted in a rectangular cavity operating in the TE₁₀₂ mode. A goniometer attached to the holder allowed precise angular rotation of the samples with respect to the external magnetic field. A standard DPPH sample was used to correct for the difference in magnetic field between the GaN sample and the gaussmeter probe (the isotropic *g*-value of DPPH is 2.0035). A P-doped Si sample was used as a standard to obtain an estimate of the density of spins associated with the EPR signals.

The crystalline quality and residual strain of the FS GaN samples were probed by X-ray diffraction and Raman scattering (RS) spectroscopy. A PANalytical X'Pert Pro X-ray diffraction (XRD) system was used to determine the full width at half maximum (FWHM) from X-ray rocking curves of the symmetric (0 0 2) and asymmetric (1 0 2) reflections. The XRD system used a CuK α_1 radiation source and a beam size of 0.5 mm \times 0.5 mm was employed. RS was performed at room temperature with the 532 nm line of a doubled Nd:YAG laser with a spot size \leq 1 μ m and detected with a micro-Raman spectrometer comprised of a microscope coupled to an Acton spectrometer equipped with a liquid nitrogen cooled CCD camera.

Room and low temperature high-resolution PL technique was used to investigate the optical properties of the GaN crystals. For the low temperature measurements (\sim 5 K), the samples were placed in a continuous flow He cryostat with temperature variation capability between 1.5 and 300 K. The luminescence was excited with the 325 nm wavelength of a He–Cd laser with an incident power between 0.7 and 0.8 mW. Neutral density filters were used to maintain the incident power within desired limits to avoid heating of the samples. The emitted light was dispersed by an 1800 groves/mm 0.85-m double-grating spectrometer and detected by a UV-sensitive GaAs photomultiplier coupled to a computer-controlled photon counter system.

The morphology of the GaN platelets was monitored by room temperature real color imaging. As excitation sources, we used the focused 325 nm laser beam of a HeCd laser with an 10–15 mW incident power and spot size \leq 100 μ m, and the white light output of the microscope lamp. The images were collected with a CCD camera coupled to an Olympus inverted microscope. Data collection was performed on the two arbitrary-labeled (due to lack of exact knowledge of the Ga and N faces) “front” of the sample and “back” of the sample surfaces using different filters and exposure times. Care was taken to optimize the collection of the emission coming from the primary surfaces and not so much from the secondary “parasitic” surfaces. All the characterization data were collected for samples in the as-grown state without any further polishing or surface conditioning.

SIMS depth profiling performed at Evans Analytical Group was used to determine the presence of impurities and their concentration levels in our samples. In particular, depth profiles for Si, O, H, C, and Li were obtained from one surface of a GaN crystal.

3. Results and discussion

3.1. XRD and Raman scattering

The crystalline quality of the GaN crystal was determined using ω -rocking curves of the symmetric (0 0 2) and asymmetric (1 0 2) reflections, where the FWHM were \sim 214 and 212 arcsec, respectively. While this crystal had grain boundaries, giving the wider FWHM values, other crystals which had been grown are of a single grain. Note that the XRD data presented here are from a randomly selected crystal from a particular growth run, which does not represent the best grown material. Measurements on different specimens from very similar growth runs occasionally produce outstanding FWHM rocking curve values of 16 arcsec [6].

Raman back-scattering data were collected at room temperature using a $z(x,xy) - z$ light polarization geometry. Measurements were performed on the front and back of the FS samples and in several positions across the sample to probe the overall crystalline quality and uniformity. The circled areas of Fig. 1a,b show the positions for the front and back surfaces where the laser was focused. The resulting first-order Raman spectra for the selected polarization of incident and scattered light are represented in the two plots of Fig. 2 as a solid line (sample front), and dashed line (sample back). Within a factor of \sim 2 difference in intensity, the results for both surfaces are identical. We observe three allowed optical phonon modes with Raman shifts at $A_1(\text{TO})=526 \text{ cm}^{-1}$, $E_2^2=564 \text{ cm}^{-1}$, and $A_1(\text{LO})=730 \text{ cm}^{-1}$. The phonon line labeled $\text{Si}(\text{TO}/\text{LO})=519 \text{ cm}^{-1}$, arises from the underlying Si substrate used to mount the GaN samples. The GaN phonon line positions appear slightly shifted. This could be attributed in part, to the use of a multimodal solid state laser for the measurements. In the future, we plan to carry out these measurements using a single mode laser. We note that for GaN, eight optical phonon modes are predicted, $1A_1(\text{TO})$, $1A_1(\text{LO})$, $2B_1$, $1E_1(\text{TO})$, $1E_1(\text{LO})$, and $2E_2$, all of which have been observed with RS, with the exception of the $2B_1$ modes which are optically inactive [7–9]. The peak positions and intense sharp lines indicate good local crystalline quality and stress-free crystals, and the $1A_1(\text{LO})$ phonon lineshape is consistent with a low free carrier concentration.

3.2. EPR

EPR is a nondestructive technique widely used to characterize point defects in bulk crystals as well as thin film semiconductors. It relies on the presence of unpaired spins whose energy levels are

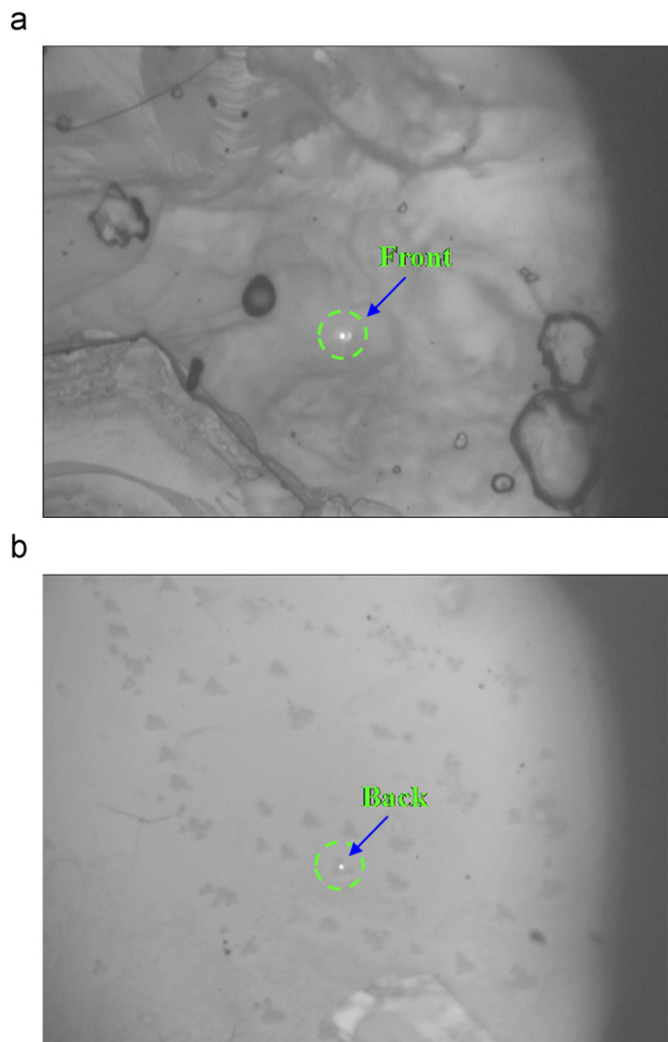


Fig. 1. (a) Front and (b) back surface micrographs of a GaN sample probed by RS. The circled areas show the positions where the 1 μm diameter laser beam was focused. In the back side, the laser was focused in a "pit".

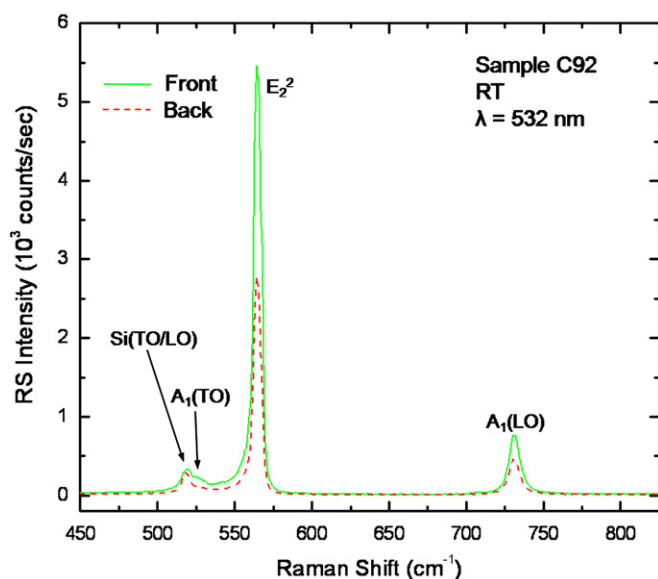


Fig. 2. Room temperature first-order Raman spectra of free-standing GaN sample.

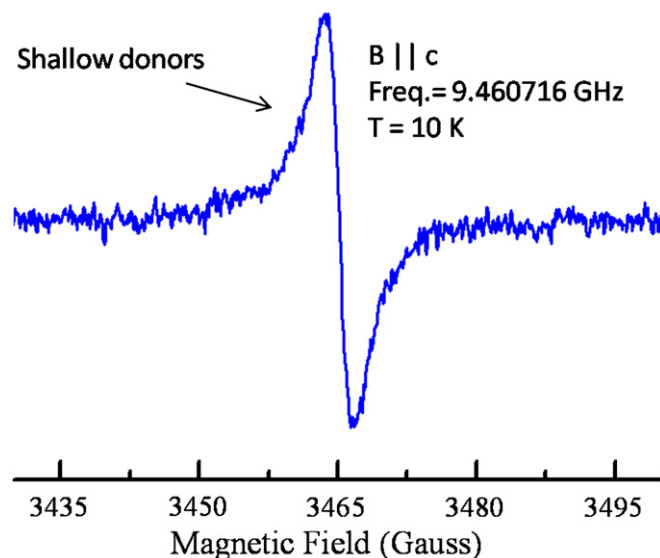


Fig. 3. Shallow donors EPR spectrum of an as-grown GaN. Data taken in the dark at 10 K, with the external magnetic field B along the $[0001]$ axis of the crystal.

split by applied external magnetic fields. Appropriate frequency perturbations will then drive the resonant transitions between these energy levels. A representative EPR spectrum from one of our as-grown GaN samples is shown in Fig. 3. This data were taken in the dark at 10 K with the external magnetic field B parallel to the c -axis of the crystal. The spectrum is characterized by a single Lorentzian resonance line with a peak-to-peak linewidth $\Delta B \approx 4.0$ Gauss and a slight anisotropy in the g -tensor with $g_{\parallel} = 1.951$ and $g_{\perp} = 1.948$ as obtained for rotations of the crystal with respect to the external magnetic field from $B \parallel [0001]$ to $B \perp [0001]$. This resonance line was assigned previously to shallow donors/conduction band electrons and attributed to Si and/or O impurities [10,11]. To the best of our knowledge, this is the first EPR observation of this shallow donor signal in bulk GaN crystals grown from solution at near atmospheric pressure. Both Si and O can act as effective-mass shallow donors in GaN when Si occupies the Ga sites and/or O the N sites. Moore et al. [12] argued in favor of the shallow character of O impurities in GaN. Conclusive identification of the shallow donors was obtained from high-resolution photoluminescence studies of undoped and Si-doped films deposited by OMCVD on HVPE-GaN, where a sharp increase on the high-energy region of the neutral donor-bound exciton in the Si-doped films was observed [13]. From the EPR standpoint alone, and due to the hydrogenic-like nature of the donors, it is not possible to discern contributions from different shallow donors in the absence of resolved nuclear hyperfine interaction.

Finally, integration of the uncompensated GaN donor EPR signal intensity and comparison with a well-calibrated Si:P standard gives an approximate concentration $\sim N_D - N_A = 3.8 \times 10^{15} \text{ cm}^{-3}$ ($\pm 50\%$).

3.3. PL

Room temperature PL spectra in the region from 1.6 to 3.6 eV are shown in Fig. 4. The PL was obtained from the front, Fig. 4a, and back, Fig. 4b of the sample. The front PL consists of a relatively sharp near band edge emission (NBE) line near 3.41 eV with a FWHM ~ 90 meV, a very weak free-to-bound band near 3.25 eV, and a dominant feature peaking near 2.45 eV with a FWHM of almost 400 meV. The photoluminescence band around 3.25 eV (see high-resolution PL inset of Fig. 4 for details) is consistent with

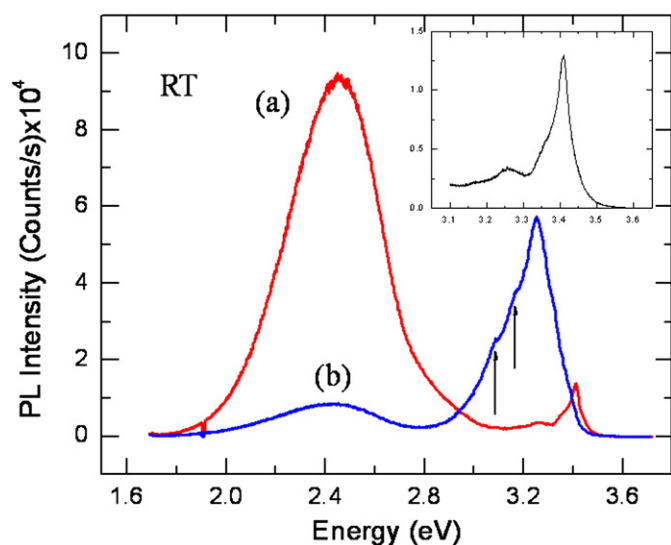


Fig. 4. Room temperature PL spectrum in the 1.6–3.6 eV spectral region. Front side (a), back side (b). Inset shows high resolution spectrum of front side in the spectral region 3.1–3.6 eV. Axis units for inset are the same as for main figure.

recombination processes involving electrons in the conduction band with holes bound to unidentified neutral shallow acceptor(s). A broad acceptor band at ~ 3.27 eV attributed to a recombination between shallow donors and shallow Mg acceptors has been observed in Mg-doped GaN epitaxial layers [14,15]. However, we do not expect Mg contamination from our growth method. The PL spectrum of the backside of the sample is dominated by the emission peaking near 3.25 eV; it is a broad band with some periodic features (discussed later), with FWHM larger than 300 meV. A much less pronounced “green” emission band at 2.45 eV is also seen. Previous investigators suggested that this green emission is intrinsic to the bulk of the material and assigned it to Ga vacancies, or Ga-vacancy-related complexes [16]. It is interesting to note that the 3.41 eV NBE band is not seen in the PL spectrum of the sample’s backside, whereas the free-to-bound emission band peaking near 3.25 eV is much stronger compared to that of the front side. When larger samples become available, we will perform additional experiments to identify the chemical nature of the acceptor(s).

The low temperature PL (5 K) results are shown in Fig. 5a,b. The spectrum obtained for the front of the sample in the region from 1.9 to 3.6 eV (with minor intensity variations, the low temperature PL spectrum from the back side in the same spectral region is similar) is characterized by an intense NBE emission line at ~ 3.47 eV and its phonon replica (labeled 1LO-NBE) at 3.37 eV. This band has previously been associated with the annihilation of free and bound excitons [17]. Also seen is the shallow donor/shallow acceptor pair (DAP) band with zero phonon line (ZPL) at 3.26 eV and phonon replicas denoted by 1LO-DAP, 2LO-DAP, and 3LO-DAP separated by ~ 92 meV, which is the energy of the $A_1(\text{LO})$ phonon. This DAP band has been previously assigned to the recombination of electrons in the shallow neutral donors with holes in the shallow neutral acceptors [18]. Therefore, the features observed in Fig. 4b with line positions at 3.092 and 3.165 eV, and denoted by arrows, are not to be confused with phonon replicas of the main line with a maximum at ~ 3.25 eV. The separation between consecutive lines is 85 and 73 meV, respectively. These results are clearly different from the expected energy separation of DAP phonon replicas. High resolution PL from the back of the sample (similar results are obtained from the front) in the NBE region is shown in Fig. 5b. It confirms the presence of a sharp

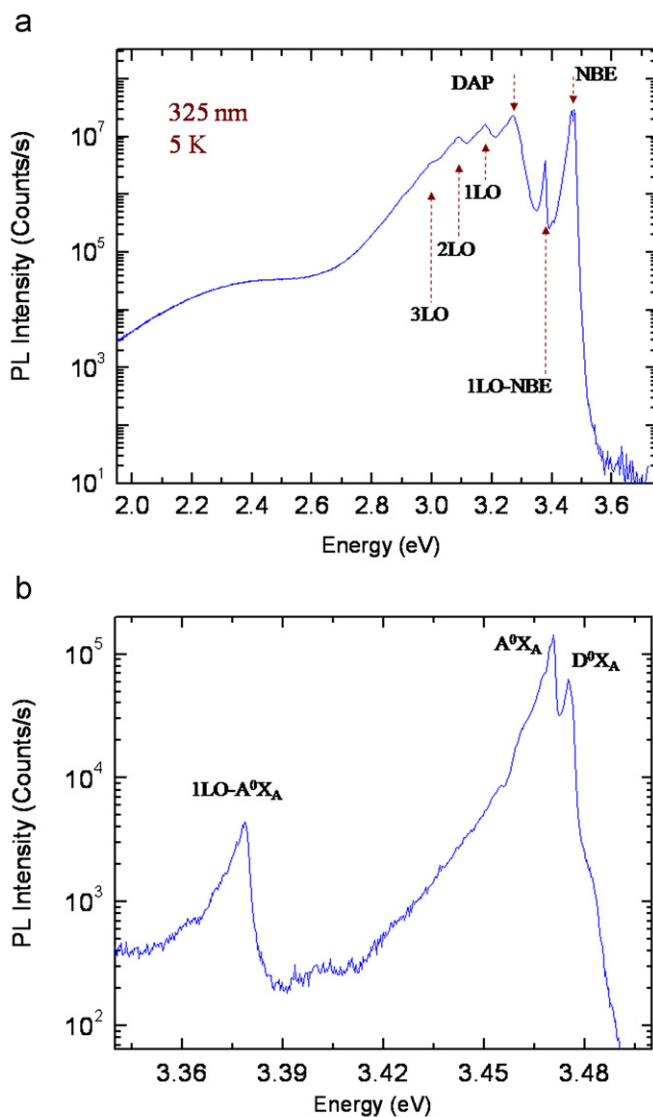


Fig. 5. (a) Low resolution PL spectrum (5 K) taken from the front side of GaN sample C92. Low incident laser power density was used to avoid heating of the sample. (b) High resolution PL spectrum (5 K) taken from the back side. Note the larger ratio of A^0X_A/D^0X_A .

donor-bound exciton (D^0X_A) at ~ 3.473 eV, and an unknown acceptor bound exciton (A^0X_A) at ~ 3.463 eV, as well as the first phonon replica 1LO- A^0X_A of the acceptor near 3.376 eV. Comparison of spectra from the back and front of the sample (not shown) in the NBE region, indicate different donor/acceptor incorporation rates, as evidenced by the intensity ratios of A^0X_A/D^0X_A PL lines. It has been reported that the PL spectrum of the Ga-face of HVPE samples show sharp peaks in the 3.28–3.5 eV spectral region, whereas the spectra from the N-face is nearly featureless due to surface damage [19]. After surface treatments, the low temperature PL spectrum from the N-face approached to that of the Ga-face [19]. These results are in good agreement with our low-temperature PL observations.

Real-color PL imaging at 300 K of the front side of the GaN sample C92 is shown in Fig. 6a,b. Fig. 6a represents the real-color (RGB) image and 6b is the fundamental contribution of the dominant green emission. These results confirm what was previously seen in the RT PL. In particular, the front side emission has a dominant band peaking near 2.45 eV (green) with a relatively strong red contribution and a weaker blue

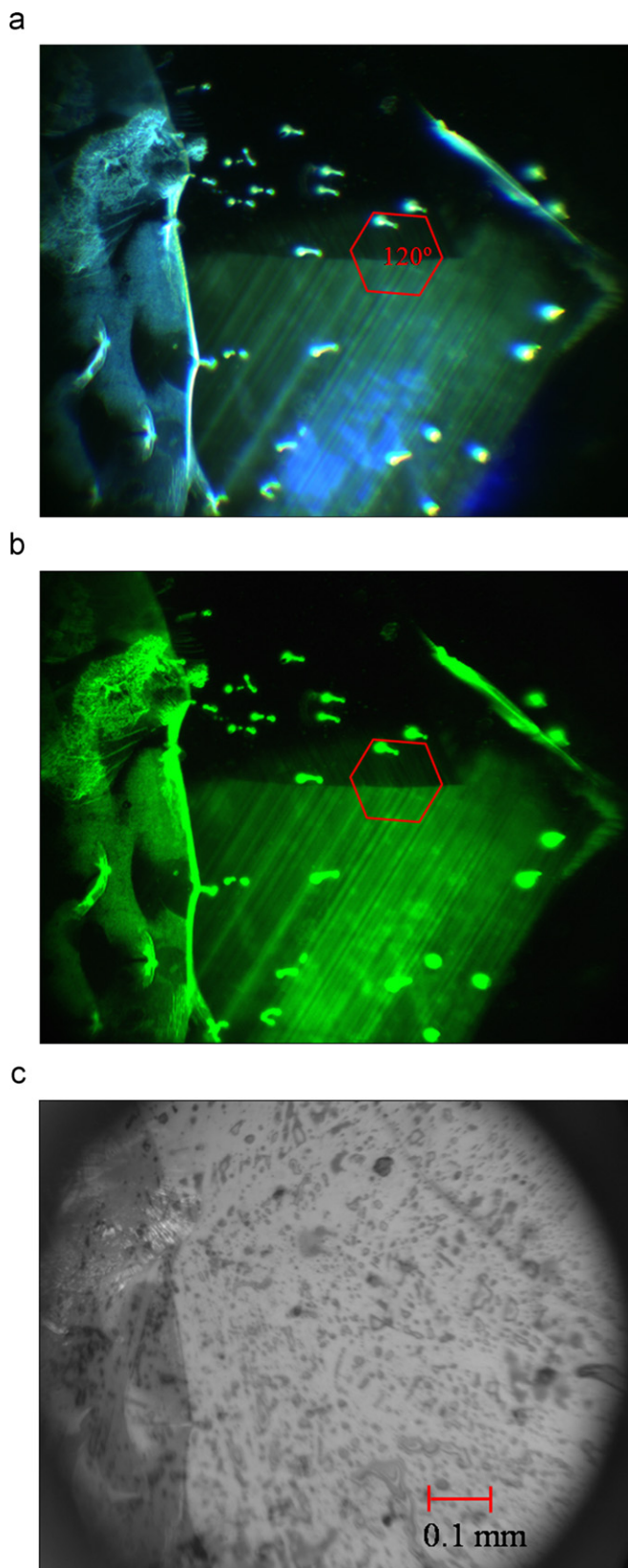


Fig. 6. Real-color (RGB) PL imaging of the front side of GaN sample C92. (a) RGB PL imaging, (b) fundamental contribution of dominant green emission, and (c) panchromatic image taken with microscope light illumination. (For interpretation of the references to color in this figure legend, the reader is referred to the web version of this article.)

emission. The images show different crystal growth sectors that manifest as a series of parallel lines of “bright” and “dark” areas with approximate equal periodicity. Two groups of lines intersecting at 120 degrees (superimposed hexagon in Fig. 6a,b is a guide to the eye to illustrate the 120° angle) appear to be in different crystal domains with a clear boundary between them. A very similar effect was observed in high-pressure high-temperature grown synthetic diamond, where a deliberate variation of the growth temperature by approximately 3 °C and an oscillation period of 22.3 min, produced areas of the crystal, called growth zoning, with equally spaced bright and dark parallel lines [20]. These authors suggested that the zoning was the result of microfluctuations of impurity concentrations in the crystal structure. We note that in naturally occurring diamonds, the very same periodic growth zoning is observed, and the concentration of defects varies from zone to zone [21,22]. The color and intensity distribution throughout our sample’s surface is not very uniform, and many areas of bright and dark spots are observed. In particular, the boundary region between intersecting planes in Fig. 6a,b, shows a drastic decrease in intensity, with the lower group of lines being more intense than the upper group. Also, randomly distributed “pits” throughout the surface show

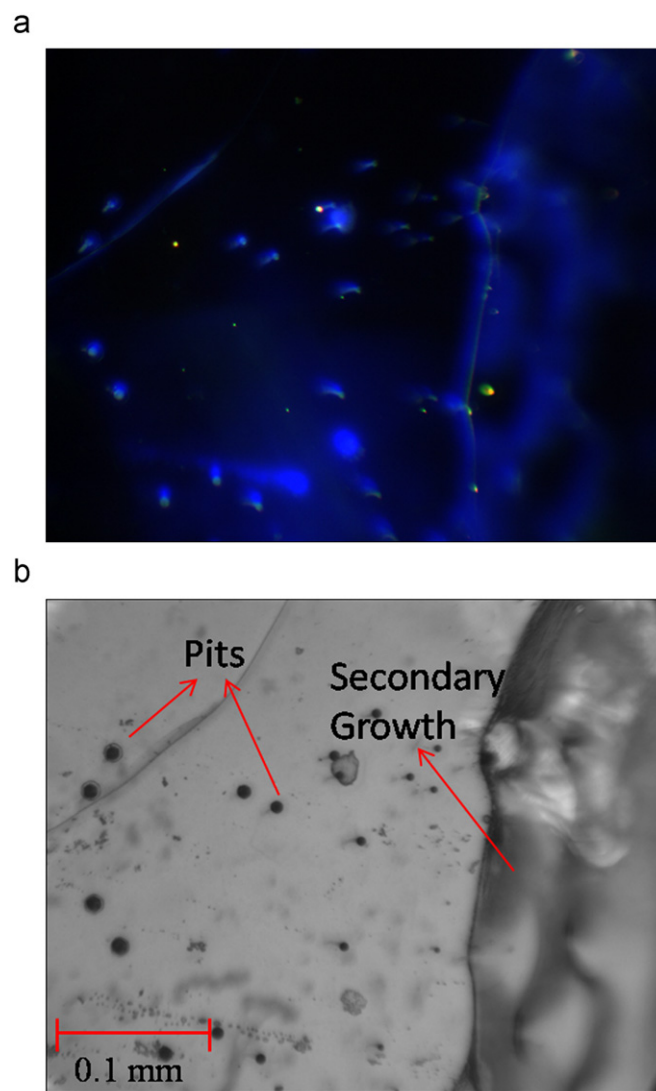


Fig. 7. Backside RGB PL (a) and panchromatic (b) micrographs.

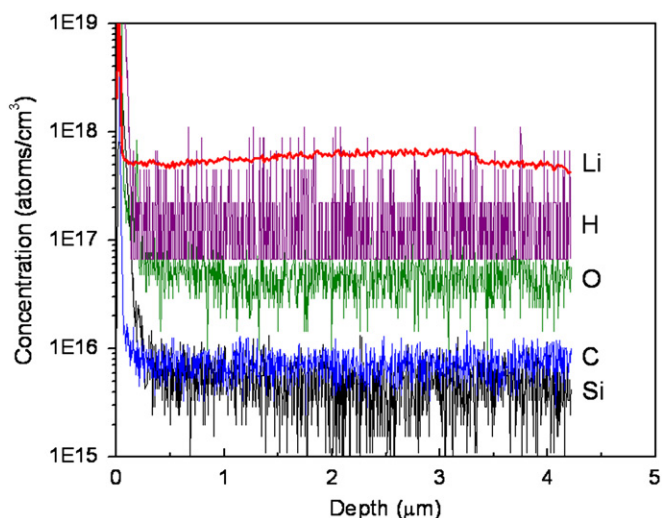


Fig. 8. SIMS depth profile measured at the front side of GaN sample C92. Li has the largest concentration, whereas O and Si are within detection limits.

brighter emissions than the primary surface. The panchromatic image taken with microscope light illumination is shown in Fig. 6c. It clearly shows an abundance of “pits” and other macroscopic defects on the surface of the sample, as well as areas of secondary “parasitic” growth. The backside RGB PL and panchromatic images are shown in Fig. 7a,b, respectively. The RGB image is dominated by blue emission (in agreement with the RT PL) with several dark areas and pits with higher emission intensity, as well as growth zoning areas similar to the ones observed on the front side, but perhaps, with different incorporation of defects and/or impurity concentrations. The red and green contributions are quite faint and in order to obtain visible images, very large acquisition times (> 300 ms) were employed. The backside panchromatic image in 7b is basically identical to that of the front side, with many visible surface defects.

3.4. SIMS

The results of SIMS depth profiling are shown in Fig. 8. The concentration levels of O and Si are $\sim 5 \times 10^{16}$ and $\sim 5 \times 10^{15}$ at/cm³, respectively. These values are close to 5×10^{16} and 5×10^{15} at/cm³, the detection limit for O and Si, respectively. Therefore, the actual O and Si concentration in our samples may be lower. These numbers are in good agreement with the estimation of total uncompensated neutral shallow donors obtained by EPR. The Li concentration level of $6\text{--}7 \times 10^{17}$ at/cm³ (SIMS detection limit $\sim 1 \times 10^{14}$ at/cm³) is not surprising since we use Li-containing precursors in our growth process and it is expected to readily dissolve in the multi-component solution. However, it is important to verify if Li is acting as an electrically active impurity, and if it is participating in any of the PL emission bands discussed here, or in emission bands in different spectral regions. For instance, when Li⁺ occupies a substitutional Ga site, it would act as a double acceptor, and it is expected to be deep. On the other hand, if Li occupies an interstitial position, it would act as a donor, but its position in the band gap is not clear. The C and H depth profiles are also shown in Fig. 8. These results are near the detection limits for these elements which are 8×10^{15} and 2×10^{17} cm⁻³, respectively. From our growth method and starting materials, we do not expect to have neither C nor H in our crystals, but cannot rule them out as possible contaminants.

Another possibility is that C and H are residual background impurities in the SIMS chamber.

4. Summary

We have presented optical and magnetic resonance results on bulk free-standing GaN single crystals grown from solution. RS indicates good local crystalline quality and stress-free crystals, and the (LO) phonon lineshape is consistent with reduced free carrier concentration. Low temperature EPR indicates that the samples have very low concentrations of shallow donors and compensating shallow acceptors. High resolution PL spectra in the NBE region show a more intense A⁰X_A line compared to the D⁰X_A line. This observation suggests a preferential incorporation of shallow acceptors in some regions of the sample. The sample's luminescence imaging is characterized by two dominant emission bands, one “green” coming from the front side, and one “blue” coming from the back side. Well-defined growth zones are observed as well, especially on the front side of the samples. This zoning is thought to be due to temperature fluctuations during crystal growth and the concentration of incorporated impurities is expected to vary within the zones. Note that not all the crystals have the “zoning” described above. Our crystals, though small at present, suggest that solution growth is a viable alternative to produce bulk GaN crystals with good optical properties and reduced concentrations of defects.

References

- [1] R. Dwilinski, R. Doradzinski, J. Garczynski, L.P. Sierzputowski, A. Puchalski, Y. Kanbara, K. Yagi, H. Minakuchi, H. Hayashi, J. Cryst. Growth 310 (2008) 3911.
- [2] R. Dwilinski, R. Doradzinski, J. Garczynski, L.P. Sierzputowski, A. Puchalski, Y. Kanbara, K. Yagi, H. Minakuchi, H. Hayashi, J. Cryst. Growth 311 (2009) 3015.
- [3] R.P. Vaudo, X. Xu, C. Loria, A.D. Salant, F.S. Flynn, G.R. Brandes, Phys. Status Solidi (a) 194 (2002) 494–497.
- [4] S. Porowski, I. Grzegory, J. Cryst. Growth 178 (1997) 174.
- [5] S. Porowski, I. Grzegory, M. Bockowski, B. Lucznik, P. Perlin, High pressure GaN crystals on HVPE GaN seeds as substrates for laser diodes, VI International Workshop on Bulk Nitride Semiconductors, August 23–28, Iznata, Poland.
- [6] B.N. Feigelson, R.M. Frazier, M. Murthy, J.A. Freitas Jr., M. Fatemi, M.A. Mastro, J.G. Tischler, J. Cryst. Growth 310 (2008) 3934.
- [7] H.W. Kunert, Cryst. Res. Technol. 38 (3–5) (2003) 366–373.
- [8] L. Bergman, M. Dutta, R.J. Nemanich, Raman Scattering in Materials Science, W.H. Weber and R. Merlin (Eds.), Springer Series in Materials Science Vol. 42, 2000, pp. 273.
- [9] J.A. Freitas Jr, M.A. Khan, Mater. Res. Soc. 339 (1994) 547.
- [10] W.E. Carlos, J.A. Freitas, M. Asif Khan, D.T. Olson, J.N. Kuznia, Phys. Rev. B 48 (1993) 17878.
- [11] N.M. Reinacher, H. Angerer, O. Ambacher, M.S. Brandt, M. Stutzmann, Mater. Res. Soc. Symp. Proc 449 (1997) 579.
- [12] W.J. Moore, J.A. Freitas Jr., G.C.B. Braga, R.J. Molnar, S.K. Lee, K.Y. Lee, I.J. Song, Appl. Phys. Lett. 79 (2001) 2570.
- [13] J.A. Freitas Jr., W.J. Moore, B.V. Shanabrook, G.C.B. Braga, S.K. Lee, S.S. Park, J.Y. Han, D.D. Koleske, J. Cryst. Growth 246 (2002) 307–314.
- [14] M. Ilegems, R. Dingle, J. Appl. Phys. 44 (1973) 4234.
- [15] E.R. Glaser, W.E. Carlos, G.C.B. Braga, J.A. Freitas Jr., W.J. Moore, B.V. Shanabrook, R.L. Henry, A.E. Wickenden, D.D. Koleske, Phys. Rev. B 65 (2002) 085312.
- [16] M.A. Reshchikov, H. Morkoc, S.S. Park, K.Y. Lee, Appl. Phys. Lett. 78 (2001) 3041.
- [17] J.A. Freitas Jr., G.C.B. Braga, W.J. Moore, J.G. Tischler, J.C. Culbertson, M. Fatemi, S.S. Park, S.K. Lee, Y. Park, J. Cryst. Growth 231 (2001) 322.
- [18] J.A. Freitas Jr., W.J. Moore, B.V. Shanabrook, G.C.B. Braga, S.K. Lee, S.S. Park, J.Y. Han, Phys. Rev. B 66 (2002) 233311.
- [19] H. Morkoc, Mater. Sci. Eng. R 33 (2001) 135–207.
- [20] Y.V. Babich, B.N. Feigelson, A.P. Yelisseyev, Diamond Relat. Mater. 13 (2004) 1802–1806.
- [21] G.P. Bulanova, J. Geochem. Explor. 53 (1995) 1–23.
- [22] E.A. Vasil'ev, S.V. Sofronev, Geol. Ore Deposits 49 (8) (2007) 784–791.